Key Engineering Materials
ISSN: 1662-9795, Vol. 926, pp 1746-1755
doi:10.4028/p-84e1pv

Submitted: 2021-12-08
Revised: 2022-02-04
Accepted: 2022-02-04
Online: 2022-07-22

Thermal Barrier Coatings (TBCs) Produced by Air Plasma Spray: Repair by Grinding and Waterjet (WJ) Processes

Luca Boccarusso[1,a*], Massimo Durante[1,b], Antonio Formisano[1,c], Antonio Langella[1,d], Fabrizio Memola Capece Minutolo[1,e]

[1]Department of Chemical Materials and Production Engineering, University of Naples Federico II, Italy

[a]luca.boccarusso@unina.it; [b]mdurante@unina.it; [c]aformisa@unina.it; [d]antgella@unina.it; [e]capece@unina.it

Keywords: Air Plasma Spray; Waterjet; Roughness; Adhesion; Repairing.

Abstract. TBCs (Thermal Barrier Coatings) are multilayer structures usually consisting of a ceramic layer, known as top coat, arranged on a connecting layer, known as bond coat, which, in turn, is arranged above the substrate to protect. These structures are applied in hot section parts of gas turbine engines for providing thermal protection. During the component life, some oxidation and/or wear phenomena can occur, therefore the TBC is generally removed and then reapplied. To simplify the manufacturing process making it more cost effectiveness, the aim of this work is to study the possibility to repair a TBC system by removing the only damaged layer by using non-conventional processes and analyzing in detail the morphological roughness to ensure a good adhesion between the layers.

Introduction

Thermal barrier coatings (TBCs) systems are multilayer structures which mainly include a thermally insulating ceramic top coat (TC), and an oxidation resistant metallic bond coat (BC). The purpose of these coating systems is to protect from the high temperature and the corrosive/oxidant environment the underlying substrate. Indeed, such TBCs are widely used as protective coatings on hot section components in advanced gas turbine engines (that represents the substrate to protect) in order to withstand increased temperatures and then improves the engine performance [1,2].

Commonly TBCs are comprised of a MCrAlY bond coat (where M is nickel, cobalt, iron or a mixture of these) and a high temperature resistant yttria-stabilized zirconia (YSZ) top coat which are applied by thermal spray on super alloys surface [2].

The most common failure during life of TBCs is due to the debonding of TC from BC caused by two main phenomena that interact with each other:

- oxidation and formation of thermally grown oxide (TGO) or infiltration of detrimental factors such as vanadium salts, which results in phase transformation and high temperature oxidation [3–5];
- thermal fatigue caused by thermal loads that arise due to the different coefficient of thermal expansion (CTE) between the ceramic top coat and the metallic bond coat [1,6].

Therefore, fatigue cracks grow in the BC/TC interface under a stress field influenced by: the mismatch between CTE of TC and BC, the roughness of the interface and the grooving of TGO. When the cracks reach a critical size, the debonding of the TC from the BC occurs, this failure mode is known as spallation.

To increase the life of these coatings, the production of a composite layer of (Al_2O_3/YSZ) coatings on BC surface is a well validated method [7]. Aluminization is the most common technique adopted for this purpose and the layer generated is known in literature as diffusion layer (DL). Indeed, due to the presence of the Al_2O_3 layer, the infiltration of oxygen or other detrimental species is prevented and the formations of TGO and zirconia phase transformation are retarded.

However, the occurring of the spallation can be postponed as much as possible but sooner or later it will be occurred. Each component with a damaged TBC must be locally repaired or globally

replaced during maintenance of the engine. This results in the engines being taken off-line for a serving period [8].

Therefore, different removal and repair techniques for damaged TBCs were studied in last years. These techniques, that mainly focused on the TC removal and its reapplication, can be summarized as follow:

- TC removal: grit blasting with abrasive method, blasting with solid CO_2, autoclaving process with caustic solutions, aqueous stripping with acid fluoride salt, Water-Jet (WJ) and Laser ablation [8,9].
- TC reapplication: Air Plasma Spray (APS), Suspension Plasma Spray (SPS), ceramic paste, ceramic gel and composite preform.

Each removal method has advantages and disadvantages, but all have to ensure the possibility to obtain a BC with an adequate surface roughness to allow the bonding of the new TC.

Therefore, in this work different types of TBCs were produced and compared in terms of bond coat roughness and adhesion strength, so the suitability of the two repairing processes (grit blasting and Water-Jet) were investigated. For this purpose, morphological analysis by using a confocal microscope and optical microscope. The results of this analysis were correlated with those obtained from tensile adhesion tests.

Materials and Methods

The base material was Inconel 718 Ni super alloy in shape of disks of 25.4 mm diameter and 5.3 mm thickness. Before TBCs production, all specimens were subjected to grit blasting using white corundum (45 mesh). The purpose of this step is to remove the oxide layer, inevitably present on the surface of the specimen, and to confer an adequate surface roughness to ensure the adhesion of the bond coat. Top and bond coat consisting of Metco 204 NS (ZrO_2-7% Y_2O_3-0.7% SiO_2-0.2% TiO_2-0.3% Al_2O_3-0.2% Fe_2O_3) and Amperit 421.761 (NiCoCrAlTaReY) respectively were obtained using APS process.

Three TBC typologies were investigated, they differ in the presence or in the type of the diffusion layer. The first TBC type (labelled as S1) was comprising of a TC bonded on a BC, this represents the easiest and basis TBC. The second and third TBC types differs from S1 for the presence of an aluminum diffusion layer (DL) on the BC. In detail for S2 type an Above Pack Cementation (APC) technique were adopted. After the production of the BC, samples were inserted in an oven for 10 hours at 1000 °C where Al-Co pallets with halides activator are present.

During this heat treatment the halides activator reacts with pellets components forming a vapor phase that transport aluminum on the surface of the BC to coat. Here, the diffusion of aluminum atoms inside the BC occurs, leading to the formation of the protective coating. Then, TC was applied.

For S3 samples, on the DL produced with APC process, an additional layer of aluminum was manually added using an In-Pack Cementation technique. It consisted in the application of a an aluminum slurry on the BC surface followed by an heat treatment under vacuum for 2 hours at 1000 °C to allow the diffusion of aluminum within the DL. Then, TC was applied.

In order to understand if and how the adhesion of TC on the underlying layer was affected by the morphology of this latter, before TC production, for each sample type roughness analyses using a 3D confocal microscope (SENSOFAR) were carried out. At this scope, four disk specimens for each sample type were used and for each specimen 20 roughness profiles were extracted and analyzed. After the roughness analyses, for each roughness parameters investigated and for each sample type, one way ANOVA tests were performed in order to understand if the measurements were statistically consistent. Microscope analyses using optical microscope (ZEISS Axioplain 2 Imaging) were carried out on both specimen cross sections and specimen top surfaces.

After the application of the TC coat, tensile adhesion tests were carried out; three disks specimens for each sample type were tested.

On sample type that showed the best mechanical performances, two stripping strategies for removing the TC were investigated: grit blasting (using a BGS Technic 8717 device) and a Water-Jet process; samples were labelled as R1 and R2 respectively. For R1, Al_2O_3 (400 mesh) were used as abrasive with a pressure of 0.3±0.03 MPa for 20 s. For R2, a pressure of 80±5 MPa at 190 mm of distance from samples and a nuzzle inclination of 45 ° were used.

After the stripping, for all specimens a morphological analysis was carried out and after the production of a new TC via APS, tensile adhesion tests were performed.

In Table 1, the processing cycle and the main experimental steps of each sample type were summarized.

Table 1. Processing cycle and experimental steps of each sample type. **For stake of brevity images at the end of the tests were not reported, but all specimens successfully passed the tests before continuing in the processing cycle.*

Experimental steps for S1	Experimental steps for S2	Experimental steps for S3
Abrasive grit blasting of substrate (white corundum 46 mesh, P=0.22 MPa, L=195 mm, α=45°)	Abrasive grit blasting of substrate (white corundum 46 mesh, P=0.22 MPa, L=195 mm, α=45°)	Abrasive grit blasting of substrate (white corundum 46 mesh, P=0.22 MPa, L=195 mm, α=45°)
Application of BC via APS (gas: Ar, H_2; cooling: air; thickness: 300 μm; powder: NiCoCrAlTaReY)	Application of BC via APS (gas: Ar, H_2; cooling: air; thickness: 300 μm; powder: NiCoCrAlTaReY)	Application of BC via APS (gas: Ar, H_2; cooling: air; thickness: 300 μm; powder: NiCoCrAlTaReY)
Aging (T=800-900 °C; t= 20 min)	Morphological analysis (Confocal microscope and optical microscope)	Morphological analysis (Confocal microscope and optical microscope)
Liquid penetrant inspection*	Application of DL via ABC (gas: Ar; cooling: Ar; Pallet: Co-Al; time: 10 h; T= 1000 °C)	Application of DL via ABC (gas: Ar; cooling: Ar; Pallet: Co-Al; time: 10 h; T= 1000 °C)
Morphological analysis (Confocal microscope and optical microscope)	Aging (T=800-900 °C; t= 20 min)	IPC on DL (slurry: Al-H_2O; Pressure: 10^{-4} MPa; cooling: Ar; time: 2h; Temperature: 1000 °C)
Application of TC via APS (gas: Ar, H_2; cooling: air; thickness: 500 μm; powder: ZrO_2-7% Y_2O_3)	Liquid penetrant inspection*	Aging (T=800-900 °C; t= 20 min)
Tensile adhesion tests	Application of TC via APS (gas: Ar, H_2; cooling: air; thickness: 500 μm; powder: ZrO_2-7% Y_2O_3)	Liquid penetrant inspection*
	Tensile adhesion tests	Application of TC via APS (gas: Ar, H_2; cooling: air; thickness: 500 μm; powder: ZrO_2-7% Y_2O_3)
		Tensile adhesion tests

Results and Discussion

In Fig. 1, typical cross section images for S1, S2 and S3 sample type before the TC deposition are reported. Comparing S1 (Fig. 1a) and S2 (Fig. 1b) it is possible to observe that the amount of porosity present in the bond coat tends to decrease after aluminization due to the occurring of diffusion mechanisms. On the other hand, the aluminization leaded a qualitative flatting of the surface and this

could obstacle the good adhesion when the TC will be applied. This aspect was also quantitatively confirmed from the roughness analysis carried out by using the confocal microscope. Apart from Ra roughness parameter (arithmetical mean height) that is very often taken into account to predict the occurrence or not of a good adhesion between the TC and the underlying layer, other roughness parameters were considered. In detail:

- Rz: Maximum height of profile;
- Rq: Root mean square deviation;
- Rp: Maximum profile peak height;
- Rv: Maximum profile valley depth;
- Rlo: Developed length of the profile;
- Rdq: Root mean square slope;
- Rsk: Skewness;
- RSm: Mean width of the profile elements.

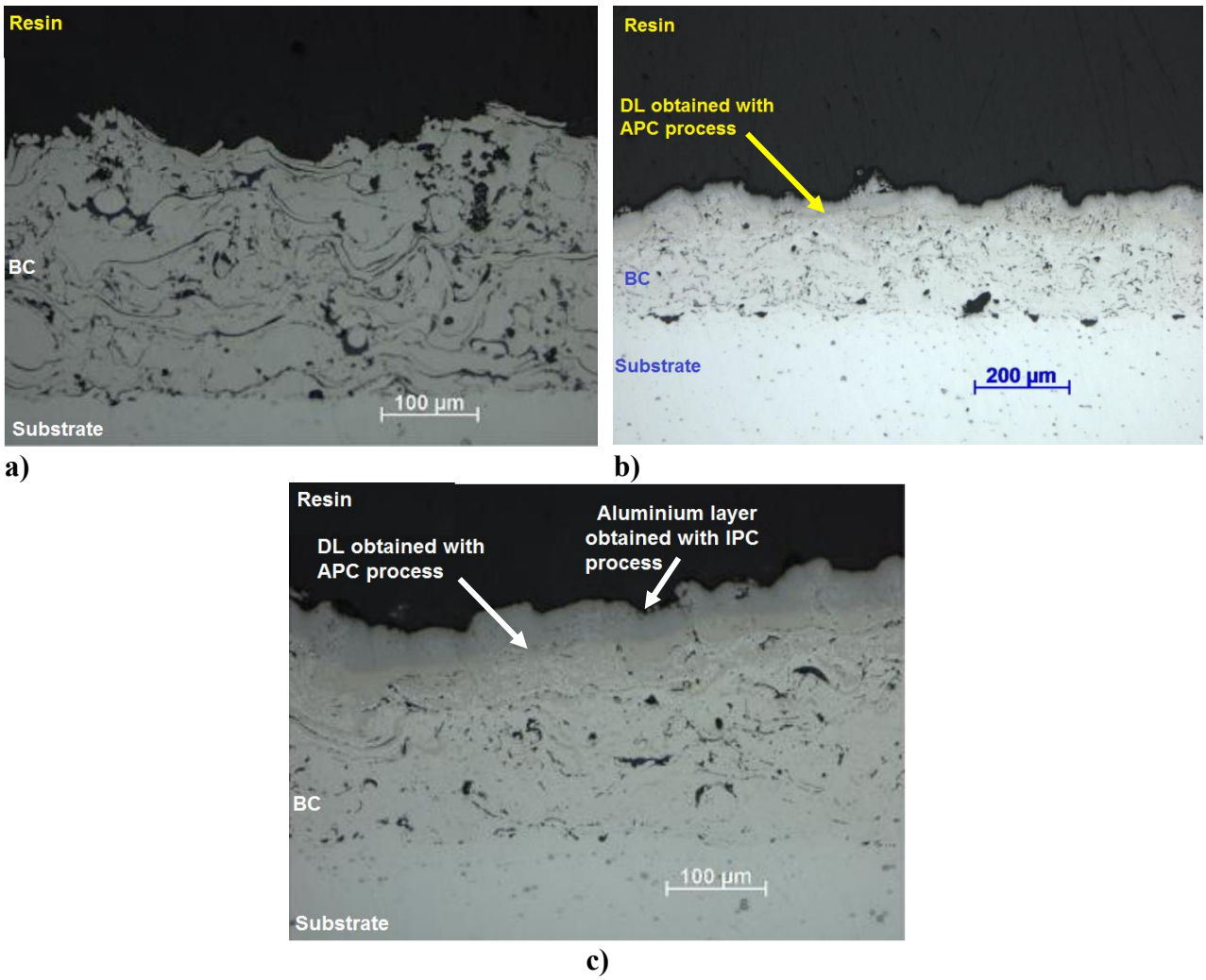

Fig. 1 Optical microscope images of the typical cross of S1 (a), S2 (b) and S3 (c) sample type.

The results of ANOVA tests showed that for all specimens of the same type the tests were successfully passed, then the measurements were statistically significant. By way of example in Fig. 2, the boxplot and the result of ANOVA test for S1 sample type for Ra are plotted. Similar results were obtained from other sample types and for each processing step.

After this step, TC was applied on the underlying layer and then tensile adhesion tests were carried out. In Fig. 3 typical cross section images for S1, S2 and S3 sample type after the TC deposition are reported and Figs. 4 and 5 shows the sample after the tensile tests and their typical upper surfaces.

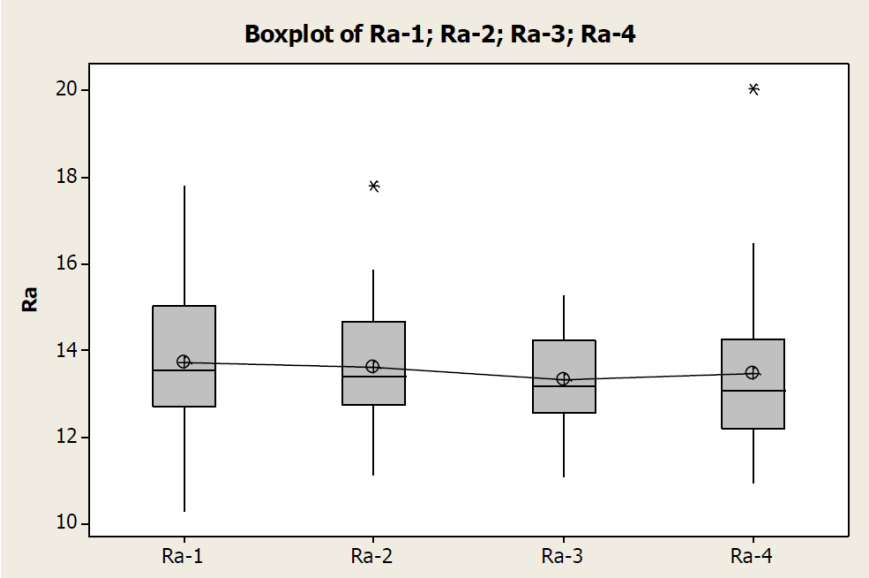

a)

One-way ANOVA: Ra-1; Ra-2; Ra-3; Ra-4

Source	DF	SS	MS	F	P
Factor	3	1,70	0,57	0,19	**0,903**
Error	76	226,39	2,98		
Total	79	228,09			

S = 1,726 R-Sq = 0,74% R-Sq(adj) = 0,00%

Individual 95% CIs For Mean Based on Pooled StDev

Level	N	Mean	StDev
Ra-1	20	13,722	1,932
Ra-2	20	13,637	1,594
Ra-3	20	13,344	1,133
Ra-4	20	13,477	2,088

```
--------+---------+---------+---------+-
        (---------------*---------------)
      (---------------*--------------)
(--------------*--------------)
  (---------------*--------------)
--------+---------+---------+---------+-
     13,00     13,50     14,00     14,50
```

Pooled StDev = 1,726

b)

Fig. 2 Box plot of Ra for sample of S1 type after the BC deposition (a) and one-way ANOVA tests results.

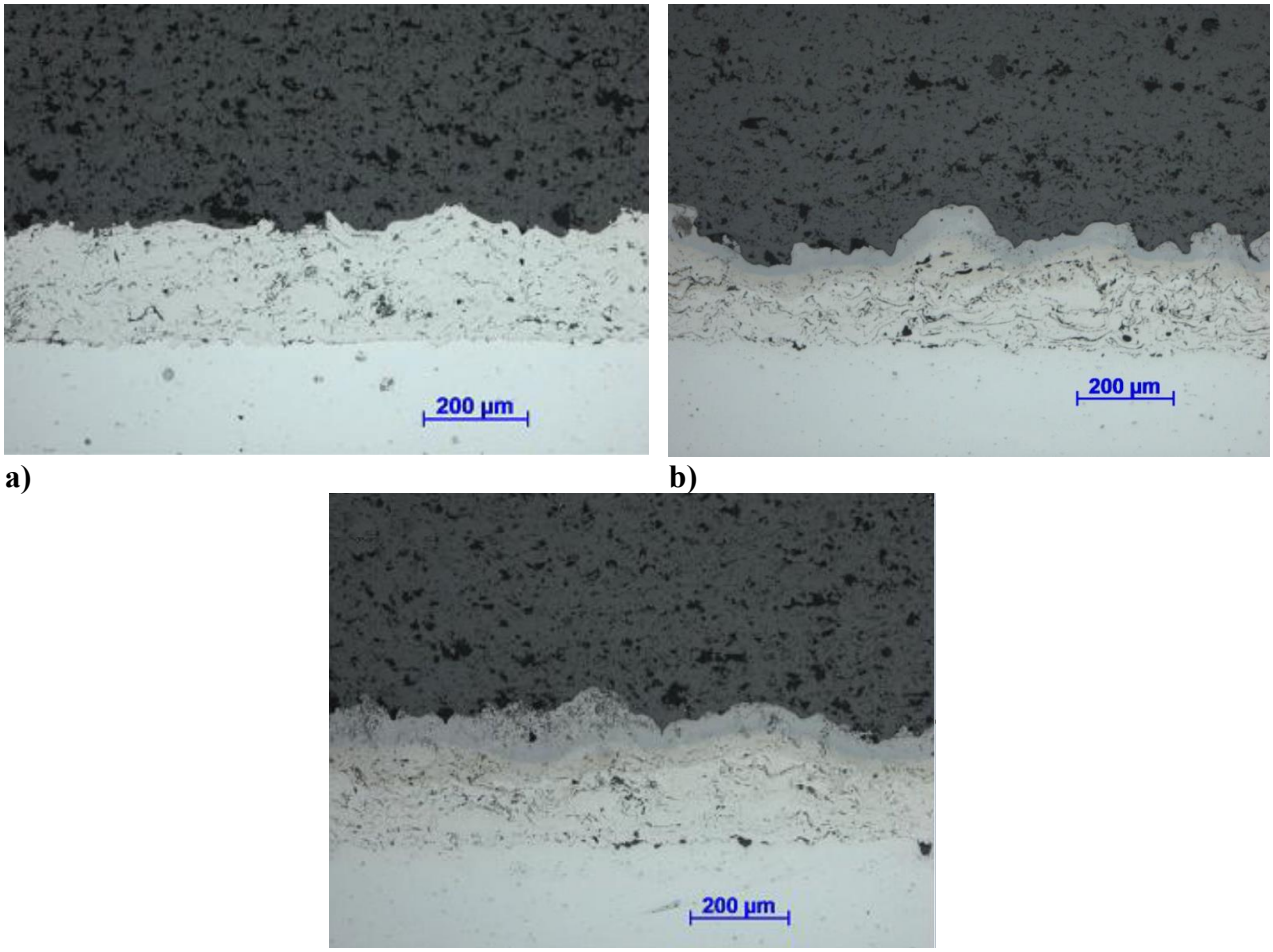

a) b)

c)

Fig. 3 Optical microscope images of the typical cross of S1 (a), S2 (b) and S3 (c) sample type.

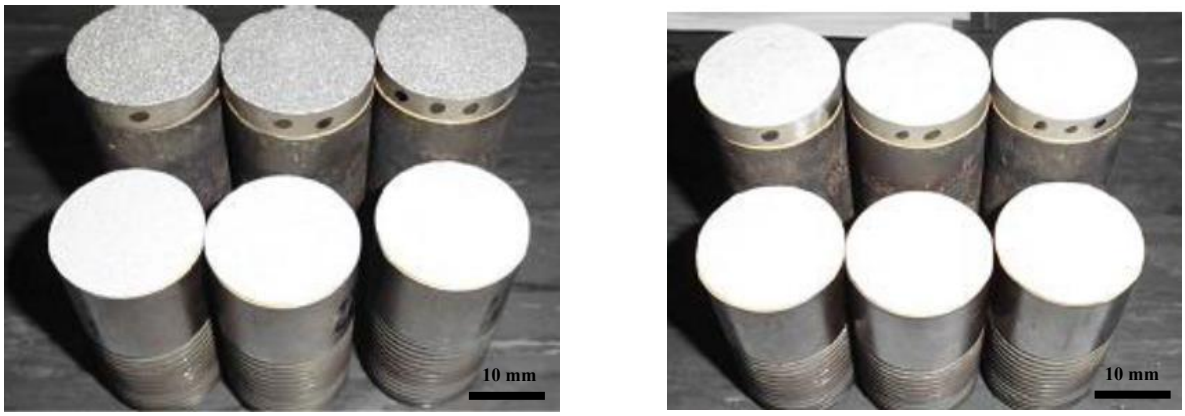

a) b)

Fig. 4 Typical specimens S1and S3 (a),and S2 (b) at the end of the tensile test.

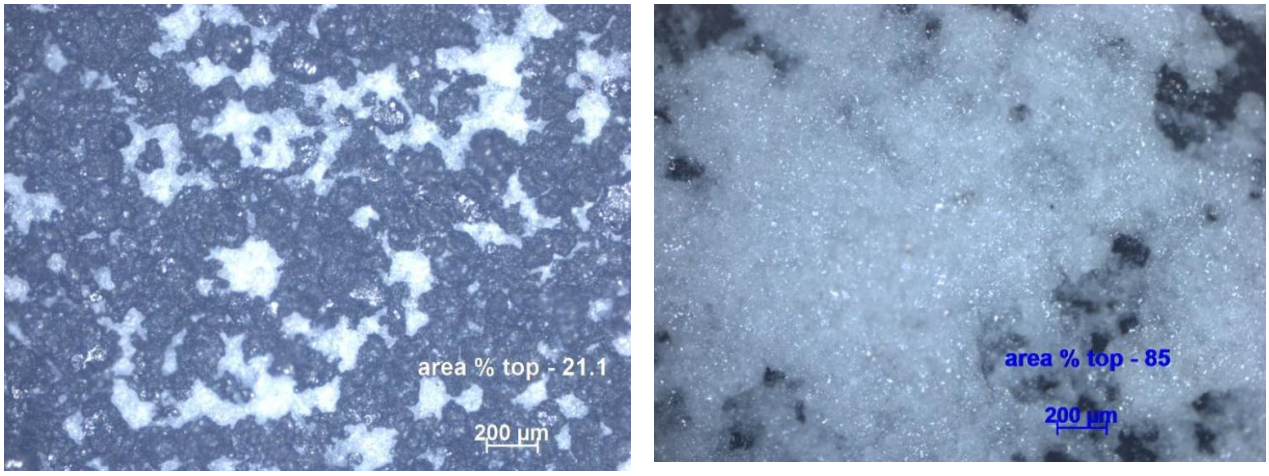

a) **b)**

Fig. 5 Typical optical images of the upper specimen surface for S1 (a) and S2 (b) sample types.

The aluminization of the bond coat obtained with the Above Pack Cementation method (S2) had the purpose of increasing the percentage of aluminum present on the surface of the bond coat in order to increase the oxidation resistance of the TBC. On the other hand, a significant reduction in the adhesion of the top coat with the underlying layer was found. This reduction was testified by comparing the tensile adhesion test results of specimens with only BC (S1) and specimens with aluminized bond coat (S2). It was found that all S2 aluminized specimens (Fig. 4b) had an adhesive failure at the interface BC/TC at values included in the range of 2.5-5 MPa, while the non-aluminized specimens (S1) showed a cohesive failure (Fig. 4a) inside the top coat with values included in the range of 10-13 MPa.

Indeed, looking at Fig. 5a it is clear that the areal percentage of the residual top coat (in white color) equal to 21.1% confirmed that the failure can be considered as adhesive. On the contrary, in Fig.5b, it was confirmed that S2 sample type showed a cohesive failure, indeed the residual area percentage of the TC was equal to 85%.

Therefore, in order to have a TBC characterized by both a good oxidation resistance and good mechanical performances, sample type S3 were produced. The major goal of the addition of the IPC step at the production cycle was the idea to make the morphology of the diffusion layer more inclined to ensure a good adhesion with the TC. Indeed, the results of the tensile tests carried out on S3 confirmed it, all S3 samples showed a cohesive failure as S2. For this reasons, S3 sample type represented the best configuration, it was able to guarantee both mechanical and oxidation resistance, so the study of the possibility to repair a damaged TBC were conducted on only this sample type. To simulate a repair, on S3 specimens the two stripping strategies were used for removing the TC and then reapplying it. In Fig. 6, typical cross section of specimen subjected to grit blasting (Fig. 6a) and Water jet stripping (Fig. 6b) was reported.

From the optical images, it was clear that the surface obtained with the grit blasting (i.e. R1 sample type) was flatter than that obtained using the WJ process (i.e. R2 sample type), this should predict a poor adhesion of the reapplied TC. Indeed, looking at Fig. 7a it is possible to note that for all samples subjected to grit blasting stripping, the top coat did not adhere on the underlying surface, differently from those obtained after the WJ stripping (see Fig.7a and b). In addition, the results of tensile tests for R2 sample type was interesting since a cohesive failure within the TC was always detected.

On the basis of these results, it is interesting to understand how the roughness morphology of the layer on which the TC is deposited can affect the final adhesion.

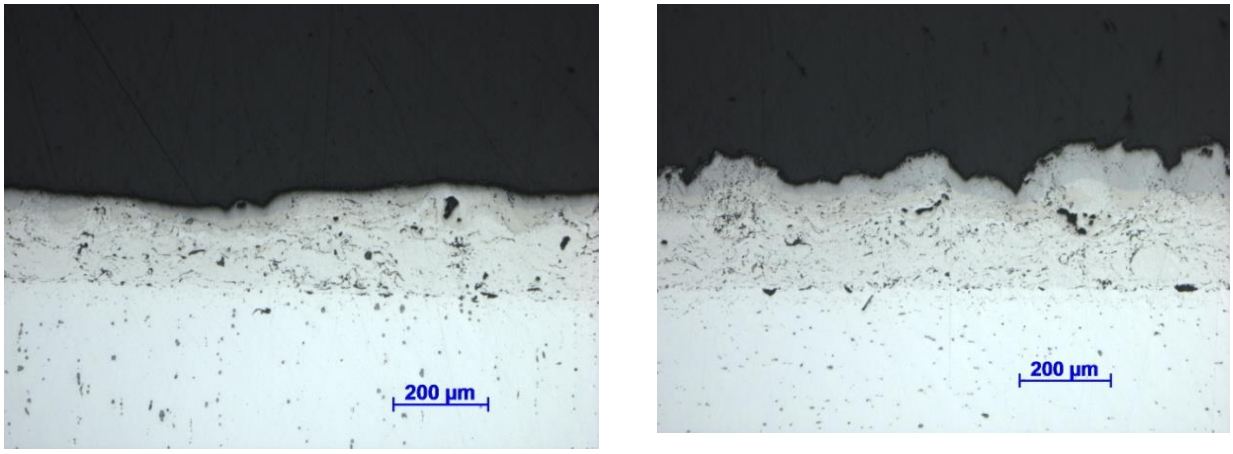

a) b)

Fig. 6 Typical cross section of sample after stripping: R1 (a) and R2 (b) sample types.

For this purpose, in Fig. 8 scatterplots of some roughness parameters vs the tensile adhesion strength were plotted (for sake of brevity only most significant roughness parameters were reported). It appears that there is not any relation between Ra and the tensile adhesion strength of the TC on the underlying layer (the same results was obtained for Rz, Rq, Rp, Rv, Rsk and RSm), vice versa a relation were found for Rlo and Rdq. There is a threshold value for both parameters (~ 27 ° for Rdq and ~ 3.56 mm for Rlo) beyond which the type of failure goes from adhesive to cohesive, so the transition from a layer with poor adhesion to a layer characterized by good adhesion with the top coat.

a)

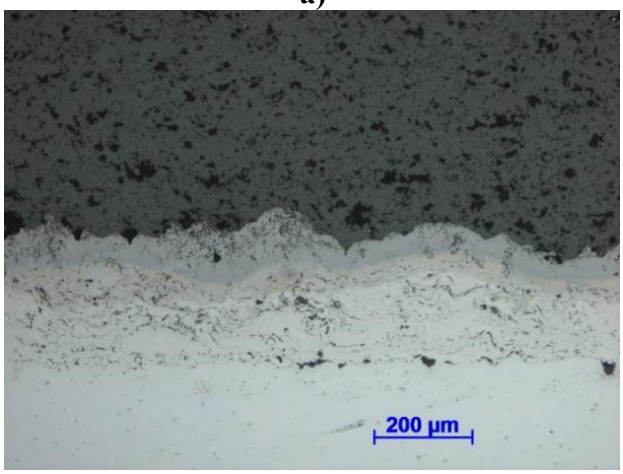

b)

Fig. 7 Specimens after reapplication of the top coat using Water Jet and grit blasting stripping technique (a) and typical cross section of sample R2 when the top cot was reapplied (b).

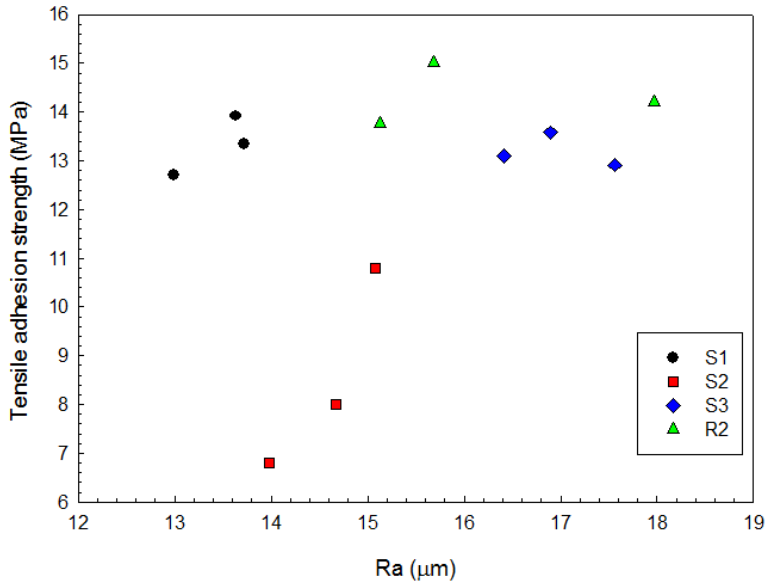

a)

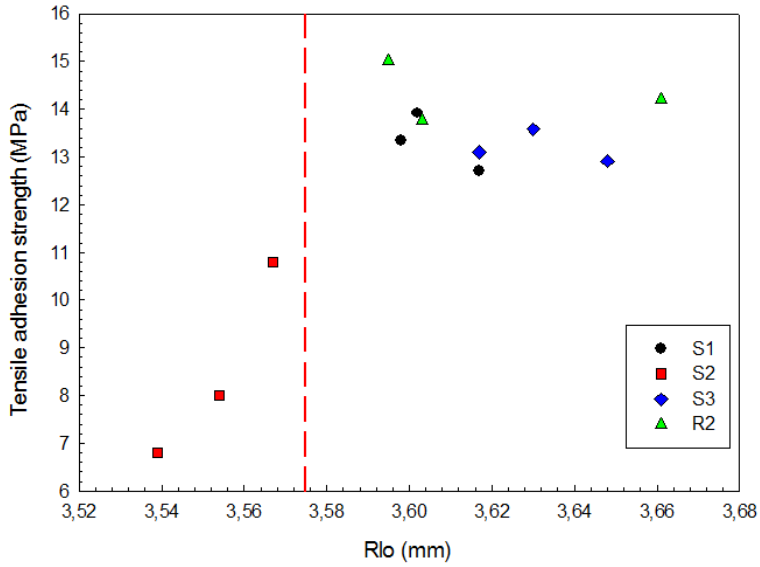

b)

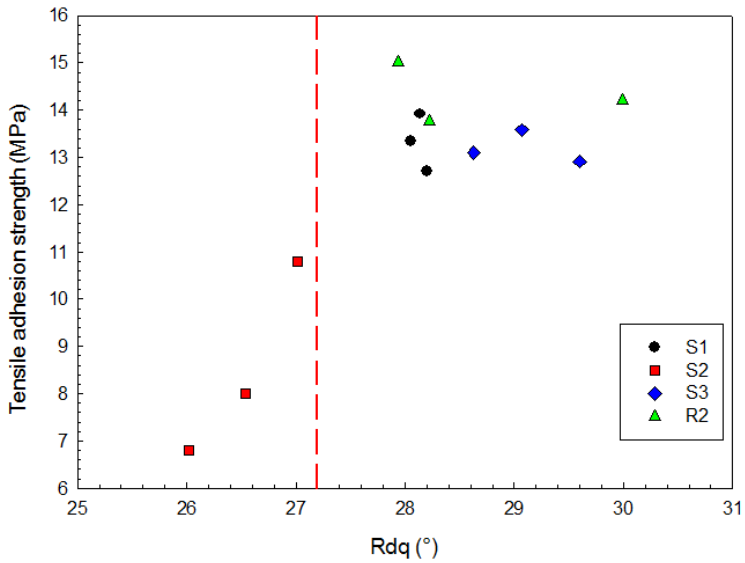

c)

Fig. 8 Scatterplot of Ra (a) Rlo (b) and Rdq (c) values vs tensile adhesion strength.

Conclusions

In the present work, three type of TBCs that mainly differ for the presence or for the type of the diffusion layer below the top coat were investigated. In detail, the study was particularly focused on the study of the roughness of the layer on which the ceramic top coat was deposited. The results showed that the measurement of the only Ra (or Rq) can not be exhaustive to understand the adhesion behavior of the top coat on the underlying layer. In fact, comparable Ra (or Rq) values were measured on samples that showed different tensile adhesion strength and different failure mode (cohesive or adhesive). Otherwise, a correlation was detected between less commonly known roughness parameters (i.e. Rdq and Rlo) and the adhesion strength, highlighting that when some threshold values were exceeded, the failure mode changes from adhesive to cohesive. Furthermore, two stripping strategy of the ceramic top coat to allow the repair of TBCs were compared: the first one based on the mechanical removal of the top coat using a grit blast technique, the second one using the Water Jet. The results showed that using the grit blasting the adhesive characteristics of the residual layer were considerably reduced so much that it was impossible to reapply the top coat. Using the Water Jet the morphological aspects was almost unchanged, allowing a successfully redeposition of a new top coat characterized by a good adhesion with the underlying layer.

References

[1] R. Eriksson, S. Sjöström, H. Brodin, S. Johansson, L. Östergren, X.H. Li, TBC bond coat-top coat interface roughness: Influence on fatigue life and modelling aspects, Surf. Coatings Technol. 236 (2013) 230–238.

[2] Y. Ozgurluk, K.M. Doleker, H. Ahlatci, A.C. Karaoglanli, Investigation of calcium–magnesium-alumino-silicate (CMAS) resistance and hot corrosion behavior of YSZ and La2Zr2O7/YSZ thermal barrier coatings (TBCs) produced with CGDS method, Surf. Coatings Technol. 411 (2021).

[3] A. Keyvani, M. Saremi, M.H. Sohi, Oxidation resistance of YSZ-alumina composites compared to normal YSZ TBC coatings at 1100 °C, J. Alloys Compd. 509 (2011) 8370–8377.

[4] M.J. Pomeroy, Coatings for gas turbine materials and long term stability issues, Mater. Des. 26 (2005) 223–231.

[5] K.M. Doleker, Y. Ozgurluk, A.C. Karaoglanli, TGO growth and kinetic study of single and double layered TBC systems, Surf. Coatings Technol. 415 (2021).

[6] M. Okazaki, S. Yamagishi, Y. Yamazaki, K. Ogawa, H. Waki, M. Arai, Adhesion strength of ceramic top coat in thermal barrier coatings subjected to thermal cycles: Effects of thermal cycle testing method and environment, Int. J. Fatigue 53 (2013) 33–39.

[7] A. Keyvani, M. Saremi, M. Heydarzadeh Sohi, Microstructural stability of zirconia-alumina composite coatings during hot corrosion test at 1050 °c, J. Alloys Compd. 506 (2010) 103–108.

[8] X. Yang, J. Zhang, Z. Lu, H.Y. Park, Y.G. Jung, H. Park, D.D. Koo, R. Sinatra, J. Zhang, Removal and repair techniques for thermal barrier coatings: a review, Trans. Inst. Met. Finish. 98 (2020) 121–128.

[9] T. Bergs, J.P. Borrmann, M. Schüler, T. Herrig, J.E. Döring, Pure waterjet controlled depth machining for stripping ceramic thermal barrier coatings on turbine blades, Procedia CIRP 85 (2020) 258–262.